

Applied Mathematics and Nonlinear Sciences

<https://www.sciendo.com>

Predicting the separation of time scales in a heteroclinic network

Maximilian Voit, Hildegard Meyer-Ortmanns[†]Department of Physics and Earth Sciences, Jacobs University Bremen, 28759 Bremen
Germany

Submission Info

Communicated by Jose Maria Amigo Garcia
Received November 26th 2018
Accepted May 3rd 2019
Available online June 28th 2019

Abstract

We consider a heteroclinic network in the framework of winnerless competition, realized by generalized Lotka-Volterra equations. By an appropriate choice of predation rates we impose a structural hierarchy so that the network consists of a heteroclinic cycle of three heteroclinic cycles which connect saddles on the basic level. As we have demonstrated in previous work, the structural hierarchy can induce a hierarchy in time scales such that slow oscillations modulate fast oscillations of species concentrations. Here we derive a Poincaré map to determine analytically the number of revolutions of the trajectory within one heteroclinic cycle on the basic level, before it switches to the heteroclinic connection on the second level. This provides an understanding of which parameters control the separation of time scales and determine the decisions of the trajectory at branching points of this network.

Keywords: winnerless competition, generalized Lotka-Volterra equations, heteroclinic dynamics, structural and temporal hierarchies
AMS 2010 codes: 37A60, 37D40.

1 Introduction

Nonlinear dynamics of heteroclinic networks is frequently found in ordinary differential equations under certain constraints like symmetries [1] or delay [2]. It is predicted in models of coupled phase oscillators [2, 3], vector models [2], pulse-coupled oscillators [4] and models of winnerless competition [5] that we consider in the following. Applications are manifold and range from social [6, 7] and ecological [5, 8] systems, to computation [4] and neuronal [9–16] networks. As it was emphasized in the work of V. Afraimovich and his coworkers [5, 9, 10, 12, 17], heteroclinic sequences in models of winnerless competition predict transient dynamics that shares features with cognitive dynamics: being simultaneously sensitive to the input and robust against perturbations. According to [17], heteroclinic dynamics may describe the binding between different information modalities in the brain (without an intrinsic hierarchy) [9], or chunking dynamics, which the brain uses to perform information

[†]Corresponding author.Email address: h.ortmanns@jacobs-university.de

processing of long sequences by splitting them into shorter information items [10]. There the hierarchy in time scales of chunking dynamics results from additional equations to the generalized Lotka-Volterra equations.

In our previous work [18] we considered a hierarchical heteroclinic network composed of a (large, superordinated) heteroclinic cycle (LHC) of three (small) heteroclinic cycles (SHCs). Each of these SHCs incorporates three saddles, corresponding to single species that temporarily survive out of the nine species in total. In [18] we have demonstrated how an appropriate choice of predation rates can steer the trajectory through the heteroclinic network in a desired way. The choice of predation rates is determined by conditions on the eigenvalues of the Jacobian at the saddles. In particular we observed a separation of time scales between the (fast) oscillations within the SHCs and the (slow) oscillations in the LHC that modulate the fast oscillations such that the scales differ by an order of magnitude. It is this aspect that is of interest in view of applications to neuronal dynamics, where a modulation of fast oscillations via slow ones is commonly observed among the multiple time scales in the brain.

In this paper we derive a Poincaré map that allows to predict how many revolutions the trajectory stays within an SHC before it switches to a heteroclinic connection of the LHC, provided that we start already in the vicinity of a saddle. The subsequent evolution of the trajectory is not covered by this map: after the switch towards a heteroclinic connection of the LHC it may either turn to a new, second SHC, or stay within the LHC. In section 2 we present the model with the choice of predation rates, in section 3 we derive the Poincaré map and present its predictions in section 4 before concluding in section 5.

2 The model

We consider a hierarchical heteroclinic network as described in [18], which consists of three small heteroclinic cycles (SHCs) that are the saddles of a large heteroclinic cycle (LHC), c.f. fig. 1. The defining equation is

$$\partial_t s_i = s_i - \gamma s_i^2 - \sum_{j \neq i} A_{i,j} s_i s_j \quad i \in \{1, \dots, 9\}, \tag{1}$$

where $s_i \in \mathbb{R}_0^+$ in the original Lotka-Volterra context denotes the concentration of species i , γ the death rate, while the set of $A_{i,j}$ constitutes the predation matrix A , which determines the topology of the heteroclinic network. For simplicity, we define the index j for given i of $A_{i,j}$ directly by the five index functions $j = es(i) = ((i + 2) \bmod 9) + 1$ (that returns the index of the expanding small direction $es(i)$), in analogy $el(i) = (i \bmod 3) + 1 + 3 \lfloor \frac{i-1}{3} \rfloor$ (expanding large), $cs(i) = es^2(i)$ (contracting small), $cl(i) = el^2(i)$ (contracting large) and $tv(i) = \{1, \dots, 9\} \setminus \{i, es(i), el(i), cs(i), cl(i)\}$ for transverse directions at saddle σ_i . The resulting topology of the hierarchical heteroclinic network is displayed in fig. 1. We set $A_{i,i} = 0$, $A_{i,cs(i)} = c$, $A_{i,cl(i)} = d$, $A_{i,es(i)} = e$, $A_{i,el(i)} = f$, and $A_{i,tv(i)} = r$. By this degeneracy of parameter values we guarantee $\mathbb{Z}_3 \times \mathbb{Z}_3$ permutation symmetry (both between species within one SHC and between the SHCs). As we have shown in [18], we can steer the trajectory along selected paths of the heteroclinic network and guarantee its stability via conditions on the eigenvalues of the Jacobian at the corresponding saddles. These conditions imply for the remaining rate parameters:

$$0 < e < f < \gamma \quad \wedge \quad c > 2\gamma - e \quad \wedge \quad d > 2\gamma - e \quad \wedge \quad r > \gamma. \tag{2}$$

An important property of eq. (1) is that the coordinate planes are invariant sets. This guarantees the existence of heteroclinic orbits. Usually such invariant planes are the result of reflection symmetries in the equations of motion. Here, such a symmetry is not manifest. However, since we restricted $s_i \geq 0$, we can extend our definition to include negative values by making the coordinate change $s_i \mapsto r_i^2$. This yields symmetric dynamics in the other $2^9 - 1$ hyperoctants, related by the reflections $\rho_i : r_i \mapsto -r_i$. In the new coordinates (and after rescaling time by a factor of 2 for convenience) the equations (1) read

$$\partial_t r_i = r_i - \gamma r_i^3 - \sum_{j \neq i} A_{i,j} r_i r_j^2 \quad i \in \{1, \dots, 9\}. \tag{3}$$

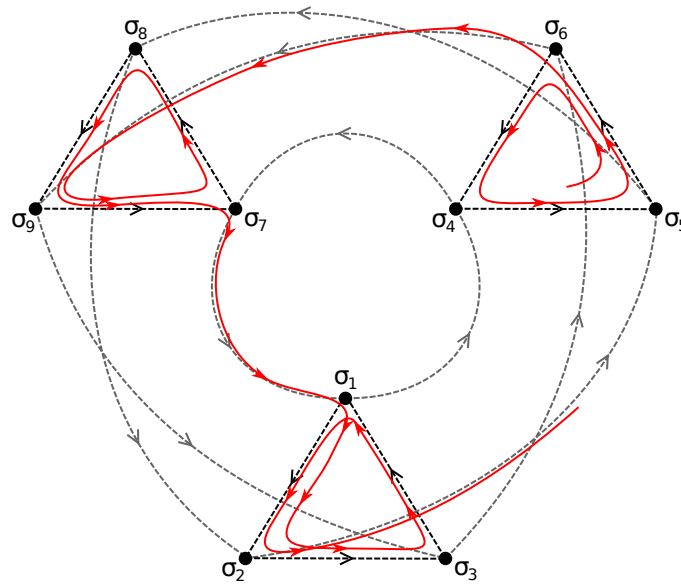


Fig. 1 Sketch of the topology of the hierarchical heteroclinic network. Black and grey dashed lines mark heteroclinic orbits with arrows indicating their directions. The red solid line gives an example for a trajectory in the vicinity of the network.

They are now equivariant under the nine reflections ρ_i , i.e., $\partial_t(\rho_k r_i) = \rho_k(\partial_t r_i)$. Due to this, the heteroclinic network is structurally stable to perturbations as long as they do not break these symmetries.

Another effect of this coordinate change is a simplification of the linearized dynamics at the saddles. The Jacobian of eq. (3), evaluated at a saddle ($r_i \neq 0 \wedge r_j = 0 \forall j \neq i$), has only entries on its diagonal, while the Jacobian of eq. (1) has additional entries in one row. In the following section we shall see why this simplification is useful.

While in all of the following we work with eq. (3), our results are still valid for the special case $s_i \geq 0 \forall i$, corresponding to eq. (1) after reversing the coordinate change.

3 Poincaré sections and return map

Our goal is to construct a Poincaré map to determine the number of revolutions in an SHC before the trajectory turns to the heteroclinic connection of the LHC. We derive the return map by proceeding in the standard way, e.g. similarly to [19]. First, we determine local maps ϕ_{abc} that characterize the dynamics in the vicinity of each saddle. Then, we argue about the form of the global maps ψ_{bc} , which transport the trajectory between the saddles' vicinities. Next, we compose local map and global map to find the transition map that describes one third of a revolution. Finally, three applications of the transition map yield the full return map.

For the local map, we linearize the dynamics at the example of saddle 1 ($r_1^* = \gamma^{-1/2}, r_j^* = 0 \forall j \neq 1$). Therefore we use local coordinates, i.e., we introduce $u_1 = r_1 - \gamma^{-1/2}$ and consider $\{u_1, r_2 \dots r_9\}$ small, so that terms of order 2 will be neglected. Thus, the linearized equations are

$$\begin{aligned}
 \partial_t u_1 &= -2u_1, & \partial_t r_2 &= (1 - \frac{\epsilon}{\gamma})r_2, & \partial_t r_3 &= (1 - \frac{\epsilon}{\gamma})r_3, \\
 \partial_t r_4 &= (1 - \frac{f}{\gamma})r_4, & \partial_t r_5 &= (1 - \frac{f}{\gamma})r_5, & \partial_t r_6 &= (1 - \frac{f}{\gamma})r_6, \\
 \partial_t r_7 &= (1 - \frac{d}{\gamma})r_7, & \partial_t r_8 &= (1 - \frac{r}{\gamma})r_8, & \partial_t r_9 &= (1 - \frac{r}{\gamma})r_9.
 \end{aligned}
 \tag{4}$$

At saddle 1, the trajectory takes one of two paths: either to saddle 2 (staying inside the SHC) or onwards to saddle 4, c.f. fig. 2(a). Each possibility is described by its own local map, ϕ_{312} and ϕ_{314} , respectively. The domain

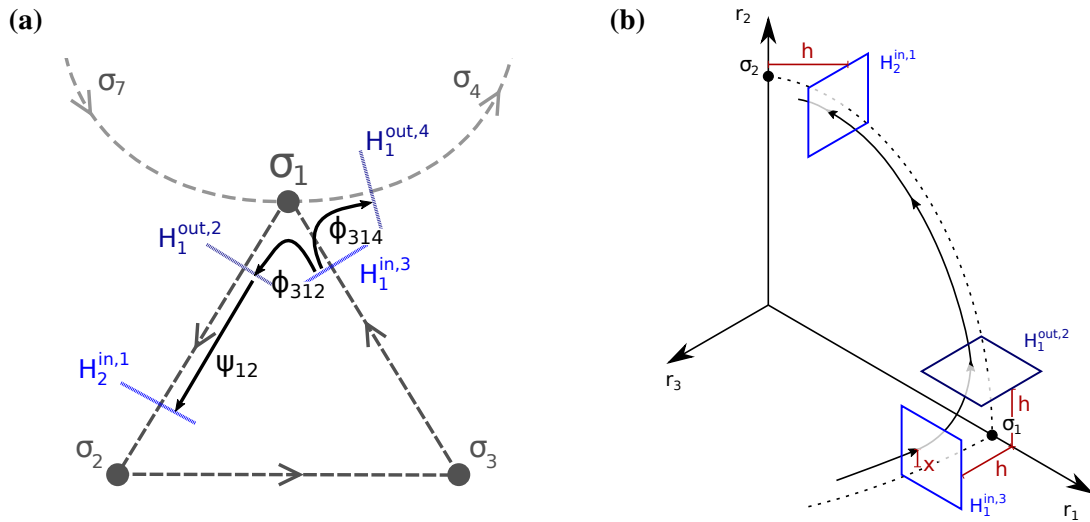


Fig. 2 (a) Schematic sketch of the vicinity of saddle σ_1 , including the cross-sections studied in section 3 together with the local maps ϕ_{312} and ϕ_{314} and the global map ψ_{12} . (b) Sketch of phase space near the saddle σ_1 showing contracting small (r_3), expanding small (r_2), and radial (r_1) directions. The solid line gives an example of a trajectory in the vicinity of the heteroclinic network. Dashed lines mark the heteroclinic orbits. While the deviation x is highlighted in this projection, y_0 cannot be visualized without the r_4 direction.

and codomains of these maps are the cross sections $H_1^{in,3} = \{(u_1, r_2 \dots r_9) : r_3 = h\}$, $H_1^{out,2} = \{(u_1, r_2 \dots r_9) : r_2 = h\}$ and $H_1^{out,4} = \{(u_1, r_2 \dots r_9) : r_4 = h\}$. The value of $h > 0$ thereby is the distance of the Poincaré sections from the saddles. It must be chosen small enough that linearizing the dynamics is justified and the local maps ϕ_{ijk} approximate the true dynamics sufficiently well. However, if h is chosen too small, the dynamics at the other side of the section is not well approximated by the linearized dynamics of the global map (see below). With respect to the $\mathbb{Z}_3 \times \mathbb{Z}_3$ symmetry, we set h the same for all cross sections without loss of generality.

We now integrate the linearized equations (4) from time T_0 of crossing $H_1^{in,3}$ to time T_1 of hitting either $H_1^{out,2}$ or $H_1^{out,4}$ (whichever is first determines the subsequent path). We use the notation $r_{i,0} = r_i(T_0)$ and $r_{i,1} = r_i(T_1)$ (and equally $u_{i,0} = u_i(T_0)$ and $u_{i,1} = u_i(T_1)$). First we focus on the local map ϕ_{312} (at σ_1 , coming from σ_3 and going to σ_2), i.e., staying in the SHC. Figure 2(b) shows a sketch. The integration yields

$$\begin{aligned} \phi_{312}(r_{1,0}, r_{2,0}, r_{3,0} = h, r_{4,0}, r_{5,0}, r_{6,0}, r_{7,0}, r_{8,0}, r_{9,0}) = & \quad (5) \\ \left((\gamma^{-\frac{1}{2}} + (r_{1,0} - \gamma^{-\frac{1}{2}})) \left(\frac{r_{2,0}}{h}\right)^{\frac{2\gamma}{\gamma-e}}, h, \left(\frac{r_{2,0}}{h}\right)^{\frac{c-\gamma}{\gamma-e}} h, \left(\frac{r_{2,0}}{h}\right)^{-\frac{\gamma-f}{\gamma-e}} r_{4,0}, \left(\frac{r_{2,0}}{h}\right)^{-\frac{\gamma-r}{\gamma-e}} r_{5,0}, \right. & \\ \left. \left(\frac{r_{2,0}}{h}\right)^{-\frac{\gamma-r}{\gamma-e}} r_{6,0}, \left(\frac{r_{2,0}}{h}\right)^{\frac{d-\gamma}{\gamma-e}} r_{7,0}, \left(\frac{r_{2,0}}{h}\right)^{-\frac{\gamma-r}{\gamma-e}} r_{8,0}, \left(\frac{r_{2,0}}{h}\right)^{-\frac{\gamma-r}{\gamma-e}} r_{9,0} \right) & \quad \text{for } \frac{\gamma-f}{\gamma-e} r_{2,0} > r_{4,0} h^{\frac{\gamma-f}{\gamma-e}-1}. \end{aligned}$$

The map ϕ_{314} looks similar, but with its fourth coordinate replaced by h (it maps to $H_1^{out,4}$) and its second coordinate by $\left(\frac{r_{4,0}}{h}\right)^{-\frac{\gamma-e}{\gamma-f}} r_{2,0} < h$. Note that the condition $\frac{\gamma-f}{\gamma-e} r_{2,0} > r_{4,0} h^{\frac{\gamma-f}{\gamma-e}-1}$, distinguishing the domains of both maps, reflects the fact that while the second coordinate of ϕ_{312} has already reached a distance h to the saddle, the fourth coordinate of ϕ_{312} , $\left(\frac{r_{2,0}}{h}\right)^{-\frac{\gamma-r}{\gamma-e}} r_{4,0}$, lags behind, so it is still smaller than h .

We abstract from this concrete case to the general local mappings $\phi_{cs(i),i,es(i)}$ utilizing the index functions from above. From eq. (5) we observe that

$$r_{i,1} = (\gamma^{-\frac{1}{2}} + (r_{i,0} - \gamma^{-\frac{1}{2}})) \left(\frac{r_{es(i),0}}{h}\right)^{\frac{2\gamma}{\gamma-e}}, \quad r_{j,1} = \left(\frac{r_{es(i),0}}{h}\right)^{-\frac{\gamma-r}{\gamma-e}} r_{j,0} \quad \forall j \in tv(i), \quad (6)$$

$$r_{es(i),1} = h, \quad r_{el(i),1} = \left(\frac{r_{es(i),0}}{h}\right)^{-\frac{\gamma-f}{\gamma-e}} r_{el(i),0}, \quad (7)$$

$$r_{cs(i),1} = \left(\frac{r_{es(i),0}}{h}\right)^{\frac{c-\gamma}{\gamma-e}} h, \quad r_{cl(i),1} = \left(\frac{r_{es(i),0}}{h}\right)^{\frac{d-\gamma}{\gamma-e}} r_{cl(i),0}. \quad (8)$$

Next, we turn to the global map $\psi_{1,2} : H_1^{\text{out},2} \rightarrow H_2^{\text{in},1}$. We will assume that $H_2^{\text{in},1}$ is reached at time T_2 , and define $r_j(T_2) = r_{j,2}$. Since the original equations (3) are equivariant under the reflections ρ_i , the global maps must as well fulfill this property, i.e., $\psi_{1,2}(\rho_i \mathbf{r}) = \rho_i \psi_{1,2}(\mathbf{r})$. More specifically: if

$$\psi_{1,2}(u_{1,1}, h, r_{3,1}, \dots, r_{j,1}, \dots, r_{9,1}) = (h, r_{2,2}, r_{3,2}, \dots, r_{j,2}, \dots, r_{9,2}), \tag{9}$$

then by equivariance we also have

$$\psi_{1,2}(u_{1,1}, h, r_{3,1}, \dots, -r_{j,1}, \dots, r_{9,1}) = (h, r_{2,2}, r_{3,2}, \dots, -r_{j,2}, \dots, r_{9,2}). \tag{10}$$

As a result, taking only lowest order terms into account we find

$$\psi_{1,2}(u_{1,1}, h, r_{3,1}, \dots, r_{9,1}) = (h, a_0 + a_1 u_{1,1} + \sum_{j \geq 3} a_j r_{j,1}^2, b_3 r_{3,1}, \dots, b_9 r_{9,1}), \tag{11}$$

for some constants a_k, b_3, \dots, b_9 . Thus, there is no ‘‘mixing’’ of variables due to the reflection symmetries (apart from the radial coordinate). Apparently \mathbb{Z}_2^n symmetries in general support the assumption that the global map acts as the identity [20]. We can thus derive the transition map $g_i = \psi_{i,es(i)} \circ \phi_{cs(i),i,es(i)}$ by describing its action on each coordinate, to find the variables r_j at time T_2 , i.e., $r_{j,2} \in H_{es(i)}^{\text{in},i}$.

$$(r_{cs(i),0})'' \equiv r_{i,2} = h, \quad (r_{cs(j),0})'' \equiv r_{j,2} = b_j r_{es(i),0}^{-\frac{\gamma-r}{\gamma-e}} r_{j,0} \quad \forall j \in tv(i), \tag{12}$$

$$(r_{i,0})'' \equiv r_{es(i),2} = f(r_{i,0}, r_{es(i),0}), \quad (r_{cs(el(i)),0})'' \equiv r_{el(i),2} = b_{el(i)} r_{es(i),0}^{-\frac{\gamma-f}{\gamma-e}} r_{el(i),0}, \tag{13}$$

$$(r_{es(i),0})'' \equiv r_{cs(i),2} = b_{cs(i)} r_{es(i),0}^{\frac{c-\gamma}{\gamma-e}} h, \quad (r_{cs(cl(i)),0})'' \equiv r_{cl(i),2} = b_{cl(i)} r_{es(i),0}^{\frac{d-\gamma}{\gamma-e}} r_{cl(i),0} \tag{14}$$

with $f(r_{i,0}, r_{es(i),0}) = a_0 + a_1 (r_{i,0} - \gamma^{-1/2}) (\frac{r_{es(i),0}}{h})^{2\gamma/E} + O(r_j^2)$. The second indices 0 and 2 represent in general the time instants before and after application of the map g_i . Upon the evolution in time, the role of the variables $r_i, i \in \{1, \dots, 9\}$ changes with respect to their directions (es, el, cs, cl). What was a $cs(i)$ -direction before the map, becomes the direction i at the subsequent saddle. Thus we apply $cs(i)$ to the indices at time T_2 (terms in the middle of eqs. (12) to (14)), using $cs(es(i)) = i, cs(cs(i)) = es(i)$, etc. This way we trace back the origin of the new directions. The arguments of the double primed terms show how the arguments transform under a generic g_i . For example, $r_{es(i),0}$ transforms to $b_{cs(i)} r_{es(i),0}^{\frac{c-\gamma}{\gamma-e}} h$, which is the new variable $r_{cs(i),2}$ assigned to the contracting small direction at time T_2 .

From eqs. (5) and (8) it seems convenient to rescale the variables r_i by h^{-1} and time by h . We thereby remove the h -dependence of the condition entering eq. (5). A short calculation with eq. (3) shows that this transformation requires to rescale all parameters (γ, c, d, e, f and r) by a factor of h^2 . To simplify the notation we introduce the new parameters

$$C = h^2(c - \gamma), \quad D = h^2(d - \gamma), \quad E = h^2(\gamma - e), \quad F = h^2(\gamma - f), \quad R = h^2(\gamma - r). \tag{15}$$

Furthermore, it is convenient to rename the variables in a way that they refer at each saddle to the same kind of direction (es, el, cs, cl , etc.). We thus identify

$$x = r_{es(i),0}, \quad y_0 = r_{el(i),0}, \quad y_n = r_{es(el(i)),0}, \quad y_p = r_{cs(el(i)),0}. \tag{16}$$

The reason why we ignore the remaining variables will become clear in eq. (20) below. The transition map, restricted to the four variables, $g_i(x, y_0, y_n, y_p) : H_i^{\text{in},cs(i)} \rightarrow H_{es(i)}^{\text{in},i}$, can now be applied repeatedly. In this way we

construct the return map $g(x, y_0, y_n, y_p) : H_i^{\text{in}, \text{cs}(i)} \rightarrow H_i^{\text{in}, \text{cs}(i)}$ by stepwise composition:

$$g_1(x, y_0, y_n, y_p) = (\hat{A}x^{\frac{C}{E}}, \hat{B}_n y_n x^{-\frac{R}{E}}, \hat{B}_p y_p x^{-\frac{R}{E}}, \hat{B}_0 y_0 x^{-\frac{F}{E}}) \tag{17}$$

$$g_2 \circ g_1(x, y_0, y_n, y_p) = (\tilde{A}x^{\frac{C}{E}^2}, \tilde{B}_p y_p x^{-\frac{R}{E} - \frac{RC}{E^2}}, \tilde{B}_0 y_0 x^{-\frac{F}{E} - \frac{RC}{E^2}}, \tilde{B}_n y_n x^{-\frac{R}{E} - \frac{FC}{E^2}}) \tag{18}$$

$$g(x, y_0, y_n, y_p) = g_3 \circ g_2 \circ g_1(x, y_0, y_n, y_p) = \tag{19}$$

$$(Ax^{\frac{C}{E}^3}, B_0 y_0 x^{-\frac{F}{E} - \frac{RC}{E^2} - \frac{RC^2}{E^3}}, B_n y_n x^{-\frac{R}{E} - \frac{FC}{E^2} - \frac{RC^2}{E^3}}, B_p y_p x^{-\frac{R}{E} - \frac{RC}{E^2} - \frac{FC^2}{E^3}}),$$

where B_0, B_n, B_p and A remain as constants. For example, the components resulting from an application of g_1 can be read off from the transition map eqs. (12) to (14) as follows: the transformation of x follows from the left equation in eq. (14), that of y_0 from the right equation in eq. (12), using the index relations for index $0 = el(i) = cs(j) = j - 1$, so that $j = el(i) + 1 = \text{index } n$, of y_n again from the right equation in eq. (12), now with $n = es(el(i)) = cs(j) = j - 1$, so that $j = el(i) + 2 = \text{index } p$, and for y_p using the right equation from eq. (13) and $p = cs(el(i))$. In the same way the actions of g_2 and g_3 can be derived.

The condition $x^{\frac{F}{E}} > y_0$ must be fulfilled at every saddle. In total this yields

$$x^{\frac{F}{E}} > y_0, \quad \hat{A}x^{\frac{CF}{E^2}} > \hat{B}_n y_n x^{-\frac{R}{E}}, \quad \tilde{A}x^{\frac{C^2 F}{E^3}} > \tilde{B}_p y_p x^{-\frac{R}{E} - \frac{RC}{E^2}} \tag{20}$$

as conditions for the domain of $g(x, y_0, y_n, y_p)$. If any condition of eq. (20) is violated, the trajectory will leave the SHC during this revolution at the respective saddle. At this point it is clear why the restriction to four variables is justified, as no other variables enter the conditions (20). All information about whether (and when) the switch to the next SHC happens is contained in x, y_0, y_n and y_p .

4 Results on the ratio between time scales

In the following, we estimate how long (in terms of revolutions) the trajectory spends near one SHC before switching to the next. Roughly three times this duration defines the time scale of an LHC. This relation defines a kind of ratio between time scales.

The idea behind the subsequent calculation is the following. Let us assume that we start at point 0 of fig. 3(a). By applying the return map g , we find the coordinates of the next point 1. The system is still in the domain of the SHC return map (below the line $x^{\frac{F}{E}}$), so that a further application of g is in order. After the n th application, the line $x^{\frac{F}{E}}$ is crossed. Here, the system switches to the next SHC.

We start by recalling the condition for following the heteroclinic connections of the SHC, given by the domain of the local map eq. (5) together with the definitions eq. (15):

$$\frac{F}{E} < \frac{\log y_0}{\log x} =: z. \tag{21}$$

Note that the relevant variable z is the ratio between orders of magnitude of the two “deviations” x and y_0 (more precisely, the distances in expanding directions from the saddles in the SHC and LHC). Every revolution corresponds to applying the return map once. From eq. (19) we find

$$\frac{\log y_0}{\log x} \mapsto \frac{\log y_0 + \beta \log x + \log B}{\alpha \log x + \log A}, \tag{22}$$

where $\alpha = \frac{C^3}{E^3}$ and $\beta = -\frac{F}{E} - \frac{RC}{E^2} - \frac{RC^2}{E^3}$, $B = B_0$ and A as before. Note that the undetermined constants A and B can be traced back to eq. (19) to the parameters b_k in eq. (11), which remain undetermined. Commonly, these constants from the global maps are either irrelevant for the result (when only stability or convergence statements should be made, as e.g. in [19, 20]), or they are determined numerically if their exact values matter for the result

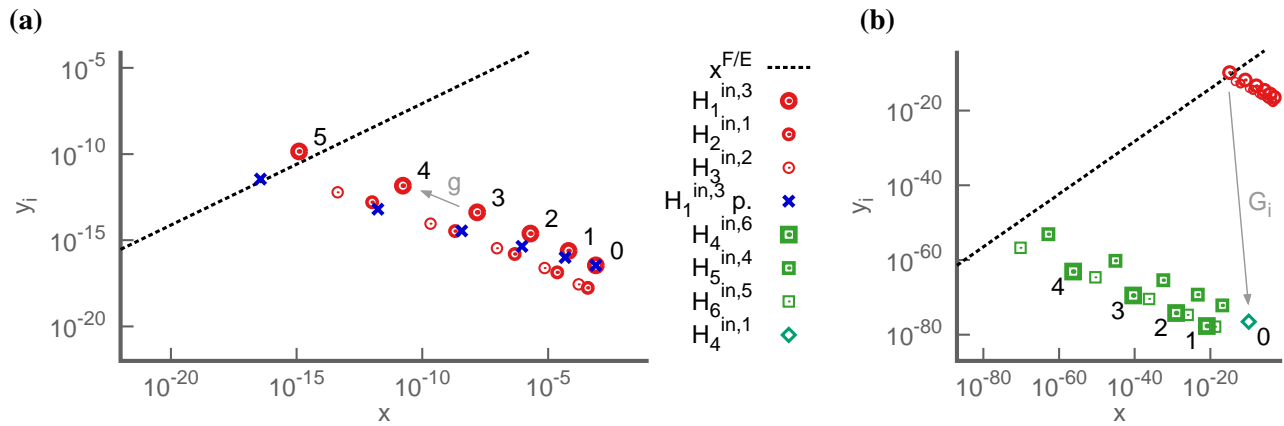


Fig. 3 (a) Plot of the coordinates $x = r_{es(i)}$ and $y_i = r_{el(i)}$ of a real trajectory when passing $H_i^{in,cs(i)} \forall i \in 1, 2, 3$ (red \odot). The dynamics switches to the subsequent SHC when the line $x = F/E$ is passed after the fifth iteration of the return map g . Blue \times mark the analytical prediction starting from point “0” assuming $A = 1 = B$ in eq. (19). When the actual coefficients $A = 1.38, B = 2.42$ (read off from the numerical data when the trajectory return to the section $H_i^{in,cs(i)}$ for the first time) are initially inserted in eq. (19), which then is iteratively applied, the analytical predictions lie precisely on top of the numerically obtained values. The small red circles below the larger ones indicate a visit of the second and third saddle within the respective SHCs. (b) Same plot as in panel (a), now including also numerical values of switches between saddles at the next SHC (green \square), together with the transition leading there (green \diamond).

(as e.g. in [21]). If we numerically determine A and B , for our choice of parameters they turn out to be of order 1. Therefore neglecting their logarithms in eq. (22), we obtain

$$\frac{\log y_0}{\log x} \mapsto \frac{\log y_0 + \beta \log x + \log B}{\alpha \log x + \log A} \approx \frac{\log y_0 + \beta \log x}{\alpha \log x} \Leftrightarrow z \mapsto \frac{1}{\alpha}(z + \beta), \quad (23)$$

with α and β as given above. We now repeatedly apply eq. (23) to eq. (21):

$$\frac{F}{E} < z \quad \rightsquigarrow \quad \frac{F}{E} < \frac{1}{\alpha}z + \frac{\beta}{\alpha} \quad \rightsquigarrow \quad \frac{F}{E} < \frac{1}{\alpha^2}z + \frac{\beta}{\alpha^2} + \frac{\beta}{\alpha} \quad \rightsquigarrow \quad \dots, \quad (24)$$

which generalizes to

$$\frac{F}{E} < \frac{1}{\alpha^n}z + \beta \frac{\alpha^{-n} - 1}{1 - \alpha}, \quad (25)$$

where we used the geometric series. Assuming equality and solving for n we find a closed expression for the approximate number of revolutions that the system stays near the SHC for given parameters and initial condition $z > F/E$:

$$n(z) = \log_{\alpha} \frac{(1 - \alpha)Ez + \beta E}{(1 - \alpha)F + \beta E}. \quad (26)$$

Note that $z \in H_i^{in,cs(i)}$ is an initial value on a cross section already near the heteroclinic network. For arbitrary initial conditions, first transient dynamics lead towards the heteroclinic network and then determine the initial values of z .

Up to now we have only taken into account y_0 and neglected the remaining conditions in eq. (20). Thus, any departure from one of the other two saddles will be perceived as the subsequent departure at saddle 1, introducing an error in n of up to $\frac{2}{3}$. To account for the other two conditions we may either repeat the above derivation accordingly and separately, starting from eq. (20); or, as we proceed in the following, transforming

the initial condition so that we start g not at σ_1 , but at σ_2 or σ_3 . We thus apply g_1 and $g_2 \circ g_1$ to (x, y_0, y_n, y_p) and deduce

$$z_1 = \frac{\log y_0}{\log x} \tag{27}$$

$$z_2 = \frac{\log \hat{B}_n y_n x^{-\frac{R}{E}}}{\log \hat{A} x^{\frac{C}{E}}} \approx \frac{E \log y_n}{C \log x} - \frac{R}{C} \tag{28}$$

$$z_3 = \frac{\log \tilde{B}_p y_p x^{-\frac{R}{E} - \frac{RC}{E^2}}}{\log \tilde{A} x^{\frac{C^2}{E^2}}} \approx \frac{E^2 \log y_p}{C^2 \log x} - \frac{ER}{C^2} - \frac{R}{C} \tag{29}$$

As a result, for any initial condition $(x, y_0, y_n, y_p) \in H_1^{\text{in},3}$ we find the number of revolutions n during which the system stays near the SHC as

$$n = \min\{n(z_1), \frac{1}{3} + n(z_2), \frac{2}{3} + n(z_3)\} \tag{30}$$

In summary, the following approximations entered our calculation: Linearization of the dynamics in the vicinity of the saddles (resulting in local maps), linearization of the global maps, and fixing the remaining constants A and B to the value 1. The justification of the linearizations as well as setting $A = B = 1$ depend on the choice of h . Note that while the distance h of Poincaré sections from the saddles cancels out of the final results (eqs. (25) and (30)), the constants A and B do depend on h . How h should be chosen so that $A = B = 1$ is a good approximation is subtle. As our tests have shown, if h is chosen too small, the approximation works less well. There is an intermediate value of h (such as $h = 0.1$) so that the Poincaré section $H_i^{\text{in},cs(i)}$ at this distance h is best located in view of applying the local map on one side of the section and the global map on the other side of the section. Otherwise the domains are not optimally located with respect to the approximations to apply. Yet, the error that is introduced by $A = B = 1$ is small ($n_{\text{pred.}} \approx 4.97$ vs. $n_{\text{num.}} \approx 5$ in fig. 3(a)). Since setting $A = B = 1$ enables the derivation of a closed expression at all, it is certainly useful to estimate the number of revolutions in this way. (It should be noticed that this number anyway fluctuates of the order of one as a function of the very initial conditions, chosen in the beginning of the time evolution, which then – after transient dynamics – lead to different initial values for z [18].)

So far the description is complete up to the point of leaving the current SHC. For the subsequent time evolution we are interested in the questions of (i) whether the system will enter the next SHC or rather continue along an LHC connection and (ii) how long (in terms of revolutions) the system will stay near the second SHC if it goes there. Again let us start at saddle σ_1 w.l.o.g. Leaving the first SHC corresponds to applying the local map ϕ_{314} and the global map ψ_{14} thereafter. However, the form of this escape map $G_1 = \psi_{14} \circ \phi_{314}$ is not covered by the generic form of g_i if it should be used for answering the former questions, though locally the condition at saddle σ_4 is the same as the first one in eq. (20) ($x^{\frac{F}{E}} > y_0$): When the trajectory approaches $H_4^{\text{out},5}$ at distance $r_5 = h$, r_7 is required to be smaller than h to continue along the LHC. However, if this prediction should be made at earlier times, from coordinates before the trajectory escapes at saddle 1 to saddle 4, the map has to keep track on $r_7 \equiv w_0$ that enters condition eq. (31)

$$\bar{B}_1 y_0^{\frac{D}{F}} w_0 < \left(\bar{A} y_0^{-\frac{R}{F}} y_n\right)^{\frac{F}{E}} \Leftrightarrow \bar{B}_1 w_0 < (\bar{A} y_n)^{\frac{F}{E}} y_0^{-\frac{R}{E} - \frac{D}{F}} \tag{31}$$

This condition can be derived from the (locally valid) condition ($x^{\frac{F}{E}} > y_0$) at saddle 4 by taking the inverse of $G_1 = \psi_{14} \circ \phi_{314}$ to obtain the coordinates prior to the escape from saddle 1. The condition (31) makes manifest the need for r_7 .

To answer the second question as to the number of revolutions within the second SHC, further coordinates r_8 and r_9 must be pursued from the beginning in order to satisfy analogous conditions to the latter two in eq. (20).

Accordingly the escape map $G_i = G_1$ depends on seven coordinates

$$G_i(x, y_0, y_n, y_p, w_0, w_n, w_p) = \left(\bar{A}y_0^{-\frac{R}{F}} y_n, \bar{B}_1 y_0^{\frac{D}{F}} w_0, \bar{B}_2 y_0^{-\frac{R}{F}} w_n, \bar{B}_3 y_0^{-\frac{R}{F}} w_p, \dots \right) \quad (32)$$

of which we worked out the four locally relevant ones: apart from y_0 , playing now the role of the former x at saddle 1, it depends on three more variables, w_0, w_n and w_p corresponding to r_7, r_8 and r_9 respectively. These are taking over the role of the former y_0, y_n and y_p , respectively, once the trajectory arrives at $H_4^{\text{out},5}$.

The escape from the first SHC, represented by G_i , is visualized in fig. 3(b), together with the following revolutions within the second SHC consisting of σ_4, σ_5 and σ_6 . It should be further noticed that revolutions within the second SHC start with ϕ_{145} , unlike subsequent visits of σ_4 where ϕ_{645} applies. Moreover, from fig. 3(b) it can be seen that the “distances” y_i of the trajectories to the LHC increase during revolutions within a single SHC, but decrease from one SHC to the next SHC, while the distances x to the heteroclinics of both SHCs decrease upon further revolutions, both results in accordance with the expectation.

5 Conclusions and Outlook

In summary, we have demonstrated how to construct a Poincaré map for a hierarchical heteroclinic network. We worked out the map in detail for predicting the number of revolutions within a small heteroclinic cycle, before the trajectory turns to the heteroclinic connection in the large cycle. The map reproduced the sensitivity to the choice of certain rate parameters that we had numerically identified in previous work as the essential ones for tuning the time scale separation between slow and fast oscillations. It also showed explicitly that the variation of the number of revolutions within an SHC depends on the initial conditions just before entering the SHC. We also indicated how to include more coordinates in the Poincaré map if its prediction should comprise further decisions of the future time evolution of the trajectory (e.g., to turn to a second and third SHC).

A detailed understanding of the time scale separation may not only be relevant for applications in neuronal dynamics, but also useful in connection with heteroclinic computing [4]. When heteroclinic computing is realized with winnerless competition, a tuned number of revolutions in a heteroclinic cycle may cause a certain amount of delay. Independently of whether the delay is desired or not, it is calculable via the Poincaré map.

If we furthermore include noise in our model of winnerless competition, it is an open and interesting question what determines the dwell time for a stay near a saddle if the saddle is a heteroclinic cycle itself. Our preliminary simulations indicate that a naive generalization of results of [2] is not applicable. According to the results of [2], the time would be determined by the logarithm of the noise intensity and the eigenvalue of the most unstable direction. Our results obtained via the Poincaré map – so far without noise – may provide a starting point for calculating the dwell time under inclusion of noise.

Acknowledgment

One of us (H.M.-O.) got inspired to work on heteroclinic networks during a talk of Valentin Afraimovich at the University of Potsdam in 2016. While working out the idea, we got into email-contact with Valentin. Valentin then invited us to present the results at the 7th International Conference on Nonlinear Science and Complexity NSC 2018 in San Luis Potosi. We appreciated very much the discussions with Valentin and dedicate this work in his memoriam. Financial support from the Deutsche Forschungsgemeinschaft DFG (contract ME-1332/28-1) is gratefully acknowledged.

References

- [1] M. Krupa, (1997), Robust Heteroclinic Cycles. *Journal of Nonlinear Science*, 7, pp. 129–176.

- [2] H. Kori and Y. Kuramoto, (2001), Slow Switching in Globally Coupled Oscillators: Robustness and Occurrence through Delayed Coupling. *Physical Review E*, 63, p. 046214.
- [3] J. Wordsworth and P. Ashwin, (2008), Spatiotemporal Coding of Inputs for a System of Globally Coupled Phase Oscillators. *Physical Review E*, 78, p. 066203.
- [4] F. Schittler Neves and M. Timme, (2012), Computation by Switching in Complex Networks of States. *Physical Review Letters*, 109, p. 018701.
- [5] V. Afraimovich, I. Tristan, R. Huerta, and M. I. Rabinovich, (2008), Winnerless Competition Principle and Prediction of the Transient Dynamics in a Lotka–Volterra Model. *Chaos: An Interdisciplinary Journal of Nonlinear Science*, 18, p. 043103.
- [6] C. Hauert and G. Szabó, (2005), Game Theory and Physics. *American Journal of Physics*, 73, pp. 405–414.
- [7] G. Szabó, J. Vukov, and A. Szolnoki, (2005), Phase Diagrams for an Evolutionary Prisoner’s Dilemma Game on Two-Dimensional Lattices. *Physical Review E*, 72, p. 047107.
- [8] M. A. Nowak and K. Sigmund, (2002), Biodiversity: Bacterial Game Dynamics. *Nature*, 418, pp. 138–139.
- [9] M. I. Rabinovich, V. S. Afraimovich, and P. Varona, (2010), Heteroclinic Binding. *Dynamical Systems*, 25, pp. 433–442.
- [10] M. I. Rabinovich, P. Varona, I. Tristan, and V. S. Afraimovich, (2014), Chunking Dynamics: Heteroclinics in Mind. *Frontiers in Computational Neuroscience*, 8, p. 00022.
- [11] M. I. Rabinovich, R. Huerta, and P. Varona, (2006), Heteroclinic Synchronization: Ultrasubharmonic Locking. *Physical Review Letters*, 96, p. 014101.
- [12] M. I. Rabinovich, R. Huerta, P. Varona, and V. S. Afraimovich, (2008), Transient Cognitive Dynamics, Metastability, and Decision Making. *PLoS Computational Biology*, 4, p. e1000072.
- [13] M. A. Komarov, G. V. Osipov, J. A. K. Suykens, and M. I. Rabinovich, (2009), Numerical Studies of Slow Rhythms Emergence in Neural Microcircuits: Bifurcations and Stability. *Chaos: An Interdisciplinary Journal of Nonlinear Science*, 19, p. 015107.
- [14] A. Szücs, R. Huerta, M. I. Rabinovich, and A. I. Selverston, (2009), Robust Microcircuit Synchronization by Inhibitory Connections. *Neuron*, 61, pp. 439–453.
- [15] M. A. Komarov, G. V. Osipov, and J. A. K. Suykens, (2009), Sequentially Activated Groups in Neural Networks. *EPL (Europhysics Letters)*, 86, p. 60006.
- [16] M. A. Komarov, G. V. Osipov, and J. A. K. Suykens, (2010), Metastable States and Transient Activity in Ensembles of Excitatory and Inhibitory Elements. *EPL (Europhysics Letters)*, 91, p. 20006.
- [17] V. S. Afraimovich, M. I. Rabinovich, and P. Varona, (2004), Heteroclinic Contours in Neural Ensembles and the Winnerless Competition Principle. *International Journal of Bifurcation and Chaos*, 14, pp. 1195–1208.
- [18] M. Voit and H. Meyer-Ortmanns, (2018), A Hierarchical Heteroclinic Network: Controlling the Time Evolution along Its Paths. *Eur. Phys. J. Spec. Top.*, 227, pp. 1101–1115.
- [19] V. Kirk and M. Silber, (1994), A Competition between Heteroclinic Cycles. *Nonlinearity*, 7, pp. 1605–1621.
- [20] S. Castro and A. Lohse, (2016), Switching in Heteroclinic Networks. *SIAM Journal on Applied Dynamical Systems*, 15, pp. 1085–1103.
- [21] T.-L. Tsai and J. H. Dawes, (2013), Dynamics near a Periodically-Perturbed Robust Heteroclinic Cycle. *Phys. Nonlinear Phenom.*, 262, pp. 14–34.